Broadband photodetection in a microfiber-graphene device

Xiaowen Sun,[1] Ciyuan Qiu,[1,*] Jiayang Wu,[1] Huanying Zhou,[1]Ting Pan,[1]Junming Mao,[1] Xi Yin,[1] Ruili Liu,[1]Weilu Gao,[2] Zheyu Fang,[3] and Yikai Su[1]

[1]State Key Lab of Advanced Optical Communication Systems and Networks, Department of Electronic Engineering, Shanghai Jiao Tong University, Shanghai 200240, China
[2]Department of Electrical and Computer Engineering, Rice University, Houston, TX77005, USA
[3]School of Physics, State Key Lab for Mesoscopic Physics, Peking University, Beijing 100871, China
**qiuciyuan@sjtu.edu.cn*

Abstract: We propose and experimentally demonstrate a microfiber-graphene device. Owing to the interaction between the graphene film and the evanescent field leaked from the microfiber, the hybrid photoconductive device exhibits a high photoresponse. A maximum photocurrent responsivity of ~2.81 mA/W is achieved in the telecommunication band. A nearly flat photoresponse spectrum within broad operational band ranging from 1500 nm to 1600 nm is also obtained as a consequence of the dispersionless and flat absorption of graphene. These results show that the proposed photocurrent generation device could provide an effective solution for broadband photodetection.

OCIS codes: (060.2310) Fiber optics; (230.5160) Photodetectors.

References and links

1. F. Bonaccorso, Z. Sun, T. Hasan, and A. C. Ferrari, "Graphene photonics and optoelectronics," Nat. Photonics **4**(9), 611–622 (2010).
2. Q. L. Bao, H. Zhang, B. Wang, Z. H. Ni, C. H. Y. X. Lim, Y. Wang, D. Y. Tang, and K. P. Loh, "Broadband graphene polarizer," Nat. Photonics **5**(7), 411–415 (2011).
3. F. Wang, Y. Zhang, C. Tian, C. Girit, A. Zettl, M. Crommie, and Y. R. Shen, "Gate-variable optical transitions in graphene," Science **320**(5873), 206–209 (2008).
4. Z. Q. Li, E. A. Henriksen, Z. Jiang, Z. Hao, M. C. Martin, P. Kim, H. L. Stormer, and D. N. Basov, "Dirac charge dynamics in graphene by infrared spectroscopy," Nat. Phys. **4**(7), 532–535 (2008).
5. M. Liu, X. Yin, E. Ulin-Avila, B. Geng, T. Zentgraf, L. Ju, F. Wang, and X. Zhang, "A graphene-based broadband optical modulator," Nature **474**(7349), 64–67 (2011).
6. M. Liu, X. Yin, and X. Zhang, "Double-Layer Graphene Optical Modulator," Nano Lett. **12**(3), 1482–1485 (2012).
7. B. Sensale-Rodriguez, R. S. Yan, M. M. Kelly, T. Fang, K. Tahy, W. S. Hwang, D. Jena, L. Liu, and H. G. Xing, "Broadband graphene terahertz modulators enabled by intraband transitions," Nat. Commun. **3**, 720 (2012).
8. Z. Sun, T. Hasan, F. Torrisi, D. Popa, G. Privitera, F. Wang, F. Bonaccorso, D. M. Basko, and A. C. Ferrari, "Graphene Mode-Locked Ultrafast Laser," ACS Nano **4**(2), 803–810 (2010).
9. D. Popa, Z. Sun, F. Torrisi, T. Hasan, F. Wang, and A. C. Ferrari, "Sub 200 fs pulse generation from a graphene mode-locked fiber laser," Appl. Phys. Lett. **97**(20), 203106 (2010).
10. Y. W. Song, S. Y. Jang, W. S. Han, and M. K. Bae, "Graphene mode-lockers for fiber lasers functioned with evanescent field interaction," Appl. Phys. Lett. **96**(5), 051122 (2010).
11. T. Mueller, F. N. A. Xia, and P. Avouris, "Graphene photodetectors for high-speed optical communications," Nat. Photonics **4**(5), 297–301 (2010).
12. X. M. Wang, Z. Z. Cheng, K. Xu, H. K. Tsang, and J. B. Xu, "High-responsivity graphene/silicon-heterostructure waveguide photodetectors," Nat. Photonics **7**(11), 888–891 (2013).
13. M. Freitag, T. Low, F. N. Xia, and P. Avouris, "Photoconductivity of biased graphene," Nat. Photonics **7**(1), 53–59 (2013).
14. F. Xia, T. Mueller, Y. M. Lin, A. Valdes-Garcia, and P. Avouris, "Ultrafast graphene photodetector," Nat. Nanotechnol. **4**(12), 839–843 (2009).
15. X. T. Gan, R. J. Shiue, Y. D. Gao, I. Meric, T. F. Heinz, K. Shepard, J. Hone, S. Assefa, and D. Englund, "Chip-integrated ultrafast graphene photodetector with high responsivity," Nat. Photonics **7**(11), 883–887 (2013).
16. M. Furchi, A. Urich, A. Pospischil, G. Lilley, K. Unterrainer, H. Detz, P. Klang, A. M. Andrews, W. Schrenk, G. Strasser, and T. Mueller, "Microcavity-Integrated Graphene Photodetector," Nano Lett. **12**(6), 2773–2777 (2012).

#245791 Received 10 Jul 2015; revised 7 Sep 2015; accepted 9 Sep 2015; published 17 Sep 2015

17. A. Pospischil, M. Humer, M. M. Furchi, D. Bachmann, R. Guider, T. Fromherz, and T. Mueller, "CMOS-compatible graphene photodetector covering all optical communication bands," Nat. Photonics **7**(11), 892–896 (2013).
18. A. K. Geim and K. S. Novoselov, "The rise of graphene," Nat. Mater. **6**(3), 183–191 (2007).
19. P. Avouris, "Graphene: Electronic and Photonic Properties and Devices," Nano Lett. **10**(11), 4285–4294 (2010).
20. R. R. Nair, P. Blake, A. N. Grigorenko, K. S. Novoselov, T. J. Booth, T. Stauber, N. M. R. Peres, and A. K. Geim, "Fine structure constant defines visual transparency of graphene," Science **320**(5881), 1308 (2008).
21. J. C. W. Song, M. S. Rudner, C. M. Marcus, and L. S. Levitov, "Hot Carrier Transport and Photocurrent Response in Graphene," Nano Lett. **11**(11), 4688–4692 (2011).
22. K. J. Tielrooij, J. C. W. Song, S. A. Jensen, A. Centeno, A. Pesquera, A. Zurutuza Elorza, M. Bonn, L. S. Levitov, and F. H. L. Koppens, "Photoexcitation cascade and multiple hot-carrier generation in graphene," Nat. Phys. **9**(4), 248–252 (2013).
23. T. Wang, X. Li, F. Liu, W. Long, Z. Zhang, L. Tong, and Y. Su, "Enhanced fast light in microfiber ring resonator with a Sagnac loop reflector," Opt. Express **18**(15), 16156–16161 (2010).
24. L. Tong, R. R. Gattass, J. B. Ashcom, S. He, J. Lou, M. Shen, I. Maxwell, and E. Mazur, "Subwavelength-diameter silica wires for low-loss optical wave guiding," Nature **426**(6968), 816–819 (2003).
25. C. Qiu, W. Gao, R. Vajtai, P. M. Ajayan, J. Kono, and Q. Xu, "Efficient Modulation of 1.55 μm Radiation with Gated Graphene on a Silicon Microring Resonator," Nano Lett. **14**(12), 6811–6815 (2014).
26. H. Lee, K. Heo, J. Park, Y. Park, S. Noh, K. S. Kim, C. Lee, B. H. Hong, J. Jian, and S. Hong, "Graphene-nanowire hybrid structures for high-performance photoconductive devices," J. Mater. Chem. **22**(17), 8372–8376 (2012).
27. C. G. Kang, S. K. Lee, S. Choe, Y. G. Lee, C. L. Lee, and B. H. Lee, "Intrinsic photocurrent characteristics of graphene photodetectors passivated with Al_2O_3," Opt. Express **21**(20), 23391–23400 (2013).
28. C. G. Kang, S. K. Lee, T. J. Yoo, W. Park, U. Jung, J. Ahn, and B. H. Lee, "Highly sensitive wide bandwidth photodetectors using chemical vapor deposited graphene," Appl. Phys. Lett. **104**(16), 161902 (2014).
29. G. Konstantatos, J. Clifford, L. Levina, and E. H. Sargent, "Sensitive solution-processed visible-wavelength photodetectors," Nat. Photonics **1**(9), 531–534 (2007).
30. C. T. Phare, Y.-H. D. Lee, J. Cardenas, and M. Lipson, "Graphene electro-optic modulator with 30 GHz bandwidth," Nat. Photonics **9**(8), 511–514 (2015).

1. Introduction

Graphene, a single atom thick carbon sheet with atoms arranged in a hexagonal structure, has attracted tremendous attentions due to its extraordinary electronic and optical properties [1]. A number of graphene-based photonic devices have been investigated [2–10]. Broadband graphene polarizer has been realized based on linear dispersion of Dirac electrons in graphene [2]. By electrically tuning the Fermi level of graphene [3, 4], high speed graphene electro-optic modulators [5, 7] were presented. Moreover, ultrafast graphene mode-locked lasers [8–10] were demonstrated by utilizing saturable absorption effect in graphene.

Graphene has been also revealed to be a promising material for photodetection [11–17]. Owing to the gapless linear dispersion of Dirac electrons in graphene [18, 19], it has a wide-band operating spectral range [20]. The two dimensional nature in graphene also makes it capable of generating multiple electron-hole pairs under light irradiation [21, 22] and converting optical signal into photocurrent or photovoltage with an external electric field. To date, several graphene-based photocurrent generation devices have been proposed and demonstrated. Nevertheless, the absorption of a monolayer graphene layer is only 2.3%. As a result, The responsivity of the graphene-based photodetector has been limited to a low level of 0.25 mA/W [13]. By applying a gate voltage on a graphene field-effect transistor (FET), the photocurrent responsivity can be improved to 0.5 mA/W [14]. Asymmetric metallization scheme has been employed to break the mirror symmetry of the internal electric-field profile in conventional graphene field-effect transistor channels, allowing for efficient photodetection with a responsivity of ~6.1 mA/W [11]. To further enhance light absorption in graphene-based photodetectors, several integration approaches have been proposed. Integrating graphene materials with a silicon waveguide [15] and Fabry-Perot microcavity [16] were demonstrated which could increase light-graphene interaction for photocurrent generation and thus improve the responsivity. In [15], Gan *et al*. demonstrated a photodetector based on a silicon waveguide with a photocurrent responsivity about 0.1 A/W while in [16], Furchi *et al*. showed a photodetector based on micro-cavity with a photocurrent responsivity about 21 mA/W.

#245791 Received 10 Jul 2015; revised 7 Sep 2015; accepted 9 Sep 2015; published 17 Sep 2015

In this letter, for the first time to the best of our knowledge, we propose and experimentally demonstrate a photocurrent generation device based on optical fiber platform. The proposed device is composed of a microfiber attached onto a graphene film connecting two metal electrodes. Benefiting from the interaction between the dispersionless graphene and light leaked from the microfiber, enhanced photocurrent responsivity can be achieved in a wide band. For an incident light at 1550 nm, the device possesses a high responsivity of ~2.81 mA/W which is limited by the high resistance from the graphene/metal contact. Based on the three-resistor model, the responsivity can be increased to be ~0.3 A/W by further reducing the resistance of the device. Experimental results also show that the device exhibits a dispersionless and flat photoresponse in a broad wavelength range from 1500 nm to 1600 nm. Compared with the existing graphene photocurrent generation devices, the proposed microfiber-graphene photocurrent generation device is advantageous low insertion loss, broadband detection, and simple fabrication.

2. Device structure, fabrication and test setup

The schematic configuration of the proposed microfiber-graphene photocurrent generation device is illustrated in Fig. 1(a). A microfiber is placed onto a graphene film, which is transferred on the gap between two Ag electrodes. The equivalent circuit of the proposed structure is depicted in Fig. 1(b). The microfiber has separated the resistance of the whole device into three parts with resistances of R_1, R_2 and R_3, respectively.

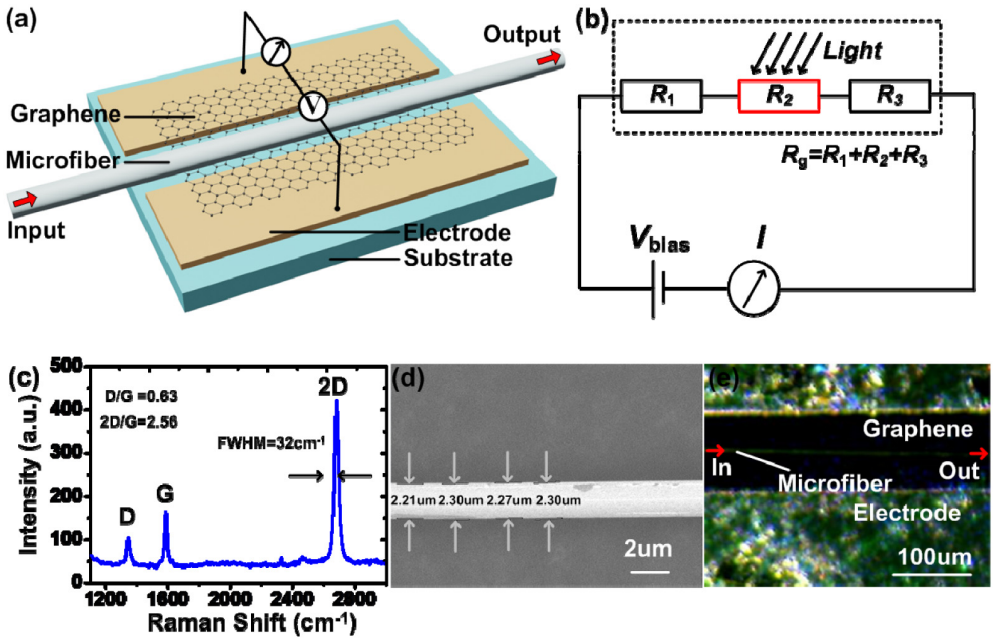

Fig. 1. (a) Schematic illustration of the proposed microfiber-graphene photocurrent generation device. (b) Equivalent circuit of the proposed structure in (a). (c) 514 nm Raman spectrum of the transferred graphene film. (d) Scanning electron microscope (SEM) image of the fabricated microfiber. (e) Micrograph of the fabricated device with microfiber attaching onto the graphene film between two Ag electrodes.

The device fabrication starts over silica substrate, and the patterned Ti (5 nm) and Ag (200 nm) electrodes is defined by photolithography, electron beam evaporation and lift-off processes. Due to the limitation of our imaging system, the gap size between the two metal electrodes is chosen to be ~100 μm to have good alignment between the microfiber and the gap. The graphene sample used in our experiment is grown by chemical vapour deposition (CVD) on Cu foil. After spinning polymethyl methacrylate (PMMA) onto the graphene

#245791 Received 10 Jul 2015; revised 7 Sep 2015; accepted 9 Sep 2015; published 17 Sep 2015

surface, the Cu foil is dissolved by $FeCl_3$ solution, and then the graphene-PMMA film is then wet transferred onto the fabricated substrate with designed patterns. Finally the PMMA is removed in acetone. The measured 514 nm Raman spectrum of the transferred graphene film is presented in Fig. 1(c), G peak and 2D peak lie at ~1586.5 cm^{-1} and ~2680.5 cm^{-1}, respectively. The 2D/G ratio is measured to be ~2.56, which indicates that the graphene used in our experiment is monolayer. The D/G ratio is ~0.63 and the full width half maximum (FWHM) of the 2D peak is ~32 cm^{-1}.

The microfiber is drawn from a commercial silica-based single mode fiber using hydrogen flame heating, similar to that in our previous work [23]. Figure 1(d) shows the scanning electron microscope (SEM) image of the fabricated microfiber, the diameter is measured to be ~2.21 μm. As shown in Fig. 1(e), the microfiber is tightly attached around the middle section of the gap by strong Van Der Waals and electrostatic forces [24] between the graphene film and microfiber. Insertion loss of the fabricated microfiber is measured to be ~1.07 dB. After placing microfiber onto the graphene film, an additional transmission loss of ~11.7 dB caused by the light-graphene interaction is observed, mainly due to the long interaction length between the graphene and the microfiber.

3. Principle and measurement results

Electron-hole pairs can be generated if the graphene film is exposed to light. To prevent recombination of the generated electron-hole pairs, applying a bias voltage between the two metal electrodes is needed to separate the photo-excited electrode-hole pairs as shown in Fig. 1(a). This results in the generation of photocurrents which depend on both the optical power in the graphene layer and the bias voltage. If the bias voltage is increased, the electrical field inside the graphene increases, thus it should be more efficiently to separate the generated electron-hole pairs and thus the photocurrent increases. Furthermore, the photocurrent also increases when the optical power in the graphene layer increases since more electro-hole pairs can be generated. To get a better idea of the optical power in the graphene layer for our proposed structure, here we characterize it from finite element calculations (COMSOL 4.3a). Figure 2(a) shows the electric field distribution of the guiding mode for the proposed structure at an operation wavelength of 1550 nm by using the Eigen-mode solver of the commercial software COMSOL. The diameter of the core of the microfiber is ~0.159 μm with a refractive index of 1.468, the diameter of the cladding of the microfiber is ~2.21 μm with a refractive index of 1.45, and the refractive index of the substrate is ~1.4. The graphene is modeled as a 1-nm-thick layer and its permittivity is calculated as follows [25]:

$$\varepsilon_g^{'}(E_f) = 1 + \frac{e^2}{8\pi E_p \varepsilon_0 d} \ln \frac{(E_p + 2|E_f|)^2 + \Gamma^2}{(E_p - 2|E_f|)^2 + \Gamma^2} - \frac{e^2}{\pi \varepsilon_0 d} \frac{|E_f|}{E_p^{\,2} + (1/\tau)^2}, \tag{1}$$

$$\begin{aligned} \varepsilon_g^{''}(E_f) = {} & \frac{e^2}{4E_p \varepsilon_0 d}\left[1 + \frac{1}{\pi}\left(\tan^{-1}\frac{E_p - 2|E_f|}{\Gamma} - \tan^{-1}\frac{E_p + 2|E_f|}{\Gamma}\right)\right. \\ & \left. + \frac{e^2}{\pi\tau E_p \varepsilon_0 d} \frac{|E_f|}{E_p^2 + (1/\tau)^2}\right], \end{aligned} \tag{2}$$

Here $\varepsilon_g^{'}$ and $\varepsilon_g^{''}$ are the real part and imaginary parts, respectively. The effective index of the micro-fiber device can thus be calculated based on the Eigen-mode solver of COMSOL. As shown in Fig. 2(a), the effective index of the micro-fiber device is analyzed if the Fermi level of the graphene is 0.4 eV [25] and the permitiviy of the graphene is 2.205 + 2.968i. The real part of the effective index n_{eff} of the micro-fiber graphene device is 1.383 while the imaginary part of n_{eff} is 6.71×10^{-4}. Here the loss of the device, determined by the imaginary part of n_{eff}, is calculated to be 118 dB/cm based on the wave propagating function as Loss = $4.34 \times 2\pi / \lambda \times$ Imag (n_{eff}). Since the measured loss of our device is 11.7 dB, the length of the device is estimated to be ~1 mm. Note that, the estimated length of the device shows small variation if

#245791 Received 10 Jul 2015; revised 7 Sep 2015; accepted 9 Sep 2015; published 17 Sep 2015

the actual Fermi level slightly deviates from 0.4 eV. By integrating the simulated electric field, the optical power in the graphene layer and the total power can be obtained. Thus the percentage of optical power in the graphene layer is obtained which is estimated to be ~0.014%. Figure 2(b) shows the dependence of the percentage of optical power in the graphene layer on the incident light wavelength for three different diameters of microfiber. One can find that less power leaks into the graphene layer when the diameter increases and thus the percentage of optical power in the graphene decrease. Furthermore, the percentage is almost constant for each fixed diameter. Since this percentage determines the absorption of the device, it indicates that the proposed device should have broad-band flat photodetection spectrum.

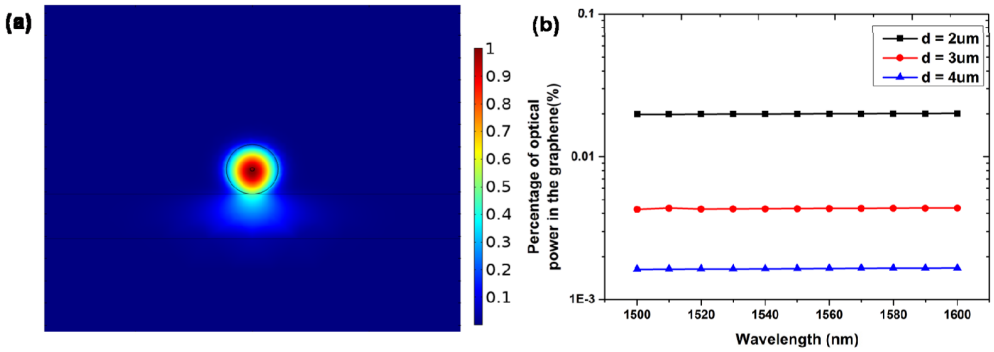

Fig. 2. (a) Electric filed distribution across microfiber-graphene structure at 1550 nm. The diameter of the micro-fiber is 2.21 μm. n_{eff} at E_f = 0.4 eV is 1.383 + 6.71e^{-4}i; (b) Dependence of the percentage of optical power in the graphene layer on the wavelength of input light.

We then monitor the I-V characteristics at different incident light powers from a tunable CW laser source (Keysight 81960A). Figure 3(a) shows the typical I-V curves of the proposed structure obtained with and without an incident light irradiated on the graphene film. Current was measured using a source meter (Keithley Instruments, model 2400). It is clear that decreased resistance of graphene can be observed when there is a 1550-nm incident light irradiated on the graphene film. We define the photocurrent generated by the light-graphene interaction as the difference between Ilight_on and Ilight_off. The photocurrents of the graphene-based microfiber structure versus bias voltage for different input power are plotted in Fig. 3(b). These results reveal that the photo-induced current depends almost linearly on the external electric field, suggesting that higher responsivities can be readily realized by applying higher bias voltages.

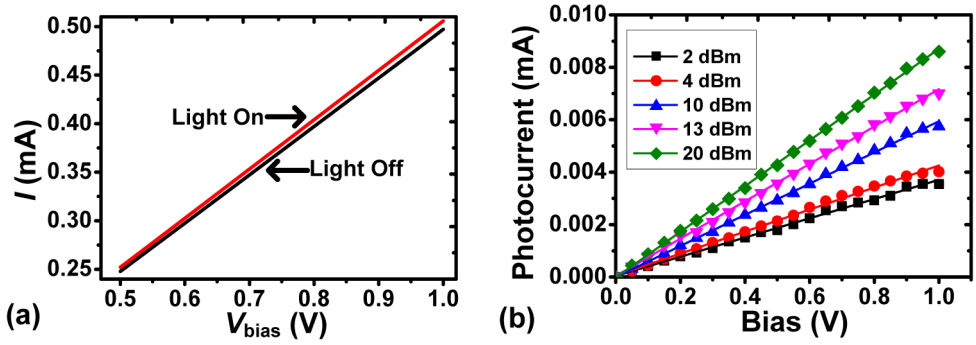

Fig. 3. (a) I-V curves of the microfiber-graphene photocurrent generation device under dark and light radiation conditions. (b) Photocurrents (I_{light_on} - I_{light_off}) as a function of applied bias voltage for different incident light powers.

#245791 Received 10 Jul 2015; revised 7 Sep 2015; accepted 9 Sep 2015; published 17 Sep 2015

Figure 4(a) depicts the generated photocurrents as a function of the incident light power at an applied bias voltage of 1 V. Here the data is plotted in log scale. One can see that the photocurrent increases with the increased incident light power. Note that the photocurrent experiences a saturation if the incident light power is about ~15 dBm with a power intensity of ~1.8 × 10^5 W/cm^2 . In the case of low incident light power, the photocurrent curve can be fitted with a simple power equation [26]:

$$\Delta I \approx AP^{\alpha}, \tag{3}$$

where A represents a constant related to a certain wavelength and P is the input light power. α is the response of the generated photocurrent to light intensity [27, 28]. The fitted result shows α = ~0.25, which is consistent with the other graphene photocurrent generation channels [27]. The low exponent obtained in our proposed device mainly comes from the defect induced by the transferred CVD graphene film and the symmetric conduction band profile in the photocurrent generation channel [26–28].

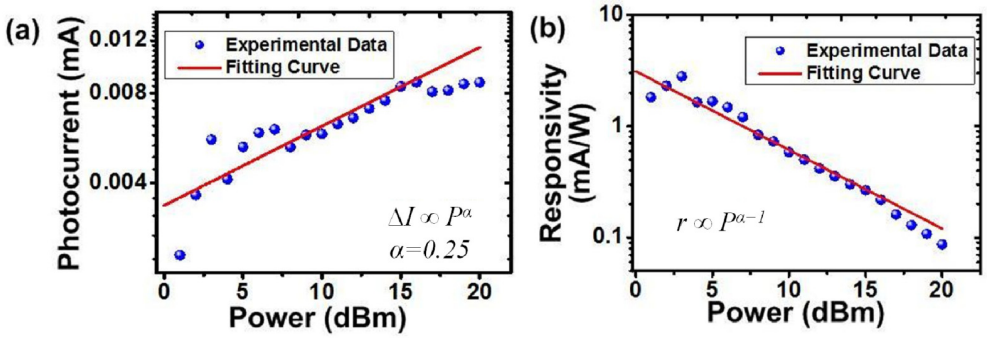

Fig. 4. (a) Photocurrents as a function of the incident light power at a bias voltage of 1 V. (b) Photocurrent responsivity versus incident light power. The proposed configuration exhibits a maximum responsivity of ~2.81 mA/W at low input power.

In order to obtain a further insight into the photocurrent generation characteristics of the proposed device, we calculated the photocurrent responsivity versus incident light power at an applied bias voltage of 1 V. Photocurrent responsivity of the device is defined as the ratio between the generated photocurrent and incident light power to the microfiber:

$$r = \frac{\Delta I}{P_{in}} = \frac{I_{ligth\_on} - I_{light\_off}}{P_{in}}. \tag{4}$$

As shown in Fig. 4(b), the photocurrent responsivity decreases with the increasing of the incident light power. A maximum responsivity of ~2.81 mA/W is measured at an excitation wavelength of 1550 nm, higher than the responsivities of conventional monolayer graphene photodetectors where the lights are irradiated on the graphene films vertically [13, 14]. The improved responsivity mainly comes from the enhanced light-graphene interaction and low insertion loss in the proposed microfiber-graphene photocurrent generation device. The noise equivalent power (NEP) can be expressed as $NEP = N / r$ where N is the noise spectral density of the device in A/$Hz^{1/2}$ and r is the responsivity in A/W. If Johnson noise dominates the noise level, N is estimated to be $N = \sqrt{4kT / R_g}$ [29]. Here k is the Boltzmann constant, T is the temperature (~300 K) and R_g the resistance of our device, which is measured to be ~2 kΩ. Since the responsivity should be larger than 2.81 mA/W if the input power decreases, NEP is estimated to be lower than 1 × 10^{-9} W/$Hz^{1/2}$. It is worth noting that the responsivity of the structure is limited by R_g. Since the sheet resistance of the graphene is about 800 Ω/square, the resistance from the graphene layer is around 80 Ω. Therefore the major part of the resistance of ~1.9 kΩ comes from the two Ag metal/graphene contacts and the metal

#245791 Received 10 Jul 2015; revised 7 Sep 2015; accepted 9 Sep 2015; published 17 Sep 2015

connections due to the oxidation of Ag in the ambient conditions. A equivalent circuit is depicted in Fig. 1(b), with three resistors shown as R_1, R_2 and R_3, respectively. R_1 and R_3 are fixed values corresponding to the resistance at the graphene/Ag contacts and the graphene resistance at the gap. R_2 is the resistance from the graphene connected to the micro fiber. Since the life time of the carriers by photoexcitation is very short, only R_2 changes its value. Assuming that the decrease in R_2 caused by light-graphene interaction is ΔR, the corresponding responsivity can be expressed as

$$r = \left(\frac{V}{R_g - \Delta R} - \frac{V}{R_g}\right) / P = \frac{V \times \Delta R}{R_g \times (R_g - \Delta R) \times P}, \tag{5}$$

where V is the applied bias voltage and R_g is the resistance of whole device which is equal to the sum of R_1,R_2 and R_3. In this experiment, R_g is about 2.012 kΩ when there is no input power. ΔR is about 22.4 Ω when the input light power is about 3 dBm. The resistance from two metal/graphene contacts could be reduced to 160 Ω [30] and the resistance from the graphene on the gap of the metal contacts could be 40 Ω by decreasing the gap to 50 μm. Thus R_g is 200 Ω which leads to a higher responsivity. By taking the advantage of long light-graphene interaction, an estimated responsivity of ~0.3 A/W could be obtained which is comparable to that in [15]. Note that, the saturation of the photoncurrent can be explained by this model. When the graphene is illuminated by the optical power with a high intensity, R_2 decreases to the minimum and the photoncurrent is saturated. Furthermore, the speed of our device could reach ~GHz based on [15].

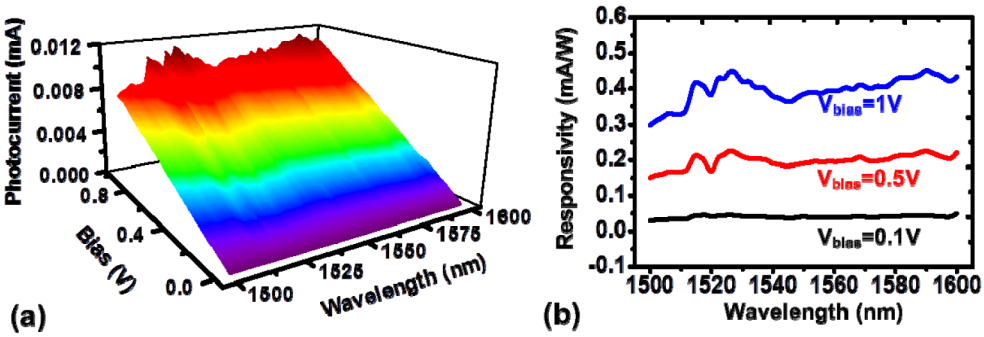

Fig. 5. (a) Experimentally measured photocurrents and (b) photocurrent responsivities at different bias voltages within a wide wavelength range from 1500 nm to 1600 nm. The incident light power was fixed at 14 dBm.

The property of flat absorption over the entire ultraviolet to far-infrared range makes graphene a potential material for ultra-broadband photodetection. Therefore, we further study the responsivity of the proposed photocurrent generation device in the near infrared wavelength range from 1500 nm to 1600 nm when the excitation power is fixed at ~14 dBm. Figure 5(a) depicts the photocurrents generated at different bias voltages as a function of the wavelength, similar to the simulation results, the photocurrent is wavelength-independent. As shown in Fig. 5(b), an approximately uniform, flat photoresponse over a wide range of wavelengths is obtained, suggesting the possibility of broadband photodetection in the microfiber-graphene device. Here the variation of the responsivity around 1520 nm might come from the fluctuation of testing system during the laser scanning process in the measurement. Broader band photodetection from 1300 nm to 1700 nm in the near infrared range is possible when the loss from fiber is low. In this experiment, it is limited by the availability of laser sources in our lab.

#245791 Received 10 Jul 2015; revised 7 Sep 2015; accepted 9 Sep 2015; published 17 Sep 2015

4. Conclusion

To summarize, we have developed a microfiber-graphene photocurrent generation device with improved photocurrent responsivity and broad detection bandwidth. The proposed device exhibits a good sensitivity to light irradiation. A maximum responsivity of ~2.81 mA/W is observed with a 1-V bias voltage at a wavelength of 1550 nm. The responsivity could be increase to be 0.3 A/W if the resistance of the device is reduced to be 200 Ω. Moreover, the experimental results verify that the presented device can operate over a wide wavelength range from 1500 nm to 1600 nm. The high responsivity and the broad detection bandwidth, together with the low insertion loss and simple fabrication, make the microfiber-graphene photocurrent generation device promising for broad-band photodetection.

Acknowledgements

This research was supported in part by the Natural Science Foundation of Shanghai under Grant 15ZR1422800, the National Natural Science Foundation of China under Grant 61125504/61235007/61422501/11374023, the 863 High-Tech Program under Grant 2015AA015503/2015AA017001, and the National Basic Research Program of China, 973 Program under Grant 2015CB932403.

#245791 Received 10 Jul 2015; revised 7 Sep 2015; accepted 9 Sep 2015; published 17 Sep 2015